MICROSTRUCTURAL ALTERATIONS IN ALUMINA CERAMICS ASSOCIATED WITH BALLISTIC IMPACT EVENTS

C. H. Kim and H. Palmour III

Technical Report 70-8 December 1970

UNDER RESEARCH PROJECT

DYNAMIC MATERIAL RESPONSE

PREPARED FOR
OFFICE OF NAVAL RESEARCH
DEPARTMENT OF THE NAVY
CONTRACT N00014-68-A-0187

62

Unclassified

Security Classification

DOCUMENT CONTROL DATA - R&D

(Security classification of title, body of abstract and indexing annotation must be entered when the overall report is classified)

1. ORIGINATING ACTIVITY *(Corporate author)*

NORTH CAROLINA STATE UNIVERSITY
Raleigh, North Carolina

2a. REPORT SECURITY CLASSIFICATION

Unclassified

2b GROUP

3. REPORT TITLE

MICROSTRUCTURAL ALTERATIONS IN ALUMINA CERAMICS ASSOCIATED WITH BALLISTIC IMPACT EVENTS

4. DESCRIPTIVE NOTES *(Type of report and inclusive dates)*

Technical Report

5. AUTHOR(S) *(Last name, first name, initial)*

Kim, Chong Hee and Palmour, H. III

6. REPORT DATE	7a. TOTAL NO. OF PAGES	7b. NO OF REFS
December, 1970	51	55

8a. CONTRACT OR GRANT NO.	9a. ORIGINATOR'S REPORT NUMBER(S)
N00014-68-A0187	
b. PROJECT NO.	70-8
c.	9b. OTHER REPORT NO(S) *(Any other numbers that may be assigned this report)*
d.	

10. AVAILABILITY/LIMITATION NOTICES

Qualified requesters may obtain copies of this report from DDC.

11. SUPPLEMENTARY NOTES	12. SPONSORING MILITARY ACTIVITY
	Office of Naval Research

13. ABSTRACT

Surface topography and defect structures associated with ballistic impact in a commercial 94 percent alumina ceramic armor are described. Fracture surfaces were examined by scanning electron microscopy, augmenting previous replication electron fractography studies. Direct transmission electron microscopy was employed in characterizing defect structures in extracted fracture fragments on replicas and in thin foils taken from bulk polycrystalline alumina in undamaged and damaged states.

A variety of dislocation interactions and tangled masses of dislocations with densities as high as 2×10^{11} cm^{-2} have been observed near intersecting surfaces in thin fracture fragments. Similar deformation textures within the bulk have been observed in impact-damaged alumina for a distance of at least 20 μm beneath a fracture surface. Localized plastic flow is most prominently evidenced in the case of cracks which are intersecting at acute angles to create fracture fragments, and in worked zones abutting propagating cracks in more massive material. These observations strongly support the concept that portions of the high stresses concentrated at the tips of propagating cracks during an impact event are relaxed by plastic deformation processes, thereby absorbing excess energy and/or delaying the fracture process to some degree.

DD FORM 1 JAN 64 1473

Unclassified

Security Classification

Unclassified
Security Classification

14 KEY WORDS	LINK A		LINK B		LINK C	
	ROLE	WT	ROLE	WT	ROLE	WT
Ceramic Armor Alumina Crystals and Ceramics Dislocations in Shocked Alumina Scanning Electron Microscopy Transmission Electron Microscopy Fracture Induced Plastic Deformation Ballistic Fracture Surface Topography Electron Diffraction Ion Beam Thinning						

INSTRUCTIONS

1. ORIGINATING ACTIVITY: Enter the name and address of the contractor, subcontractor, grantee, Department of Defense activity or other organization *(corporate author)* issuing the report.

2a. REPORT SECURITY CLASSIFICATION: Enter the overall security classification of the report. Indicate whether "Restricted Data" is included. Marking is to be in accordance with appropriate security regulations.

2b. GROUP: Automatic downgrading is specified in DoD Directive 5200.10 and Armed Forces Industrial Manual. Enter the group number. Also, when applicable, show that optional markings have been used for Group 3 and Group 4 as authorized.

3. REPORT TITLE: Enter the complete report title in all capital letters. Titles in all cases should be unclassified. If a meaningful title cannot be selected without classification, show title classification in all capitals in parenthesis immediately following the title.

4. DESCRIPTIVE NOTES: If appropriate, enter the type of report, e.g., interim, progress, summary, annual, or final. Give the inclusive dates when a specific reporting period is covered.

5. AUTHOR(S): Enter the name(s) of author(s) as shown on or in the report. Enter last name, first name, middle initial. If military, show rank and branch of service. The name of the principal author is an absolute minimum requirement.

6. REPORT DATE: Enter the date of the report as day, month, year; or month, year. If more than one date appears on the report, use date of publication.

7a. TOTAL NUMBER OF PAGES: The total page count should follow normal pagination procedures, i.e., enter the number of pages containing information.

7b. NUMBER OF REFERENCES: Enter the total number of references cited in the report.

8a. CONTRACT OR GRANT NUMBER: If appropriate, enter the applicable number of the contract or grant under which the report was written.

8b, 8c, & 8d. PROJECT NUMBER: Enter the appropriate military department identification, such as project number, subproject number, system numbers, task number, etc.

9a. ORIGINATOR'S REPORT NUMBER(S): Enter the official report number by which the document will be identified and controlled by the originating activity. This number must be unique to this report.

9b. OTHER REPORT NUMBER(S): If the report has been assigned any other report numbers *(either by the originator or by the sponsor)*, also enter this number(s).

10. AVAILABILITY/LIMITATION NOTICES: Enter any limitations on further dissemination of the report, other than those imposed by security classification, using standard statements such as:

(1) "Qualified requesters may obtain copies of this report from DDC."

(2) "Foreign announcement and dissemination of this report by DDC is not authorized."

(3) "U. S. Government agencies may obtain copies of this report directly from DDC. Other qualified DDC users shall request through

_____."

(4) "U. S. military agencies may obtain copies of this report directly from DDC. Other qualified users shall request through

_____."

(5) "All distribution of this report is controlled. Qualified DDC users shall request through

_____."

If the report has been furnished to the Office of Technical Services, Department of Commerce, for sale to the public, indicate this fact and enter the price, if known.

11. SUPPLEMENTARY NOTES: Use for additional explanatory notes.

12. SPONSORING MILITARY ACTIVITY: Enter the name of the departmental project office or laboratory sponsoring *(paying for)* the research and development. Include address.

13. ABSTRACT: Enter an abstract giving a brief and factual summary of the document indicative of the report, even though it may also appear elsewhere in the body of the technical report. If additional space is required, a continuation sheet shall be attached.

It is highly desirable that the abstract of classified reports be unclassified. Each paragraph of the abstract shall end with an indication of the military security classification of the information in the paragraph, represented as *(TS), (S), (C), or (U)*.

There is no limitation on the length of the abstract. However, the suggested length is from 150 to 225 words.

14. KEY WORDS: Key words are technically meaningful terms or short phrases that characterize a report and may be used as index entries for cataloging the report. Key words must be selected so that no security classification is required. Identifiers, such as equipment model designation, trade name, military project code name, geographic location, may be used as key words but will be followed by an indication of technical context. The assignment of links, roles, and weights is optional.

Unclassified
Security Classification

NORTH CAROLINA STATE UNIVERSITY
Raleigh, North Carolina

MICROSTRUCTURAL ALTERATIONS IN ALUMINA CERAMICS ASSOCIATED WITH BALLISTIC IMPACT EVENTS

C. H. Kim and H. Palmour, III

Technical Report 70-8

December 1970

Prepared for

Office of Naval Research
Contract N00014-68-A-0187
(NR 064-504)

1 September 1967 - 31 August 1973

under a project entitled

DYNAMIC MATERIAL RESPONSE

ABSTRACT

Surface topography and defect structures associated with ballistic impact in a commercial 94 percent alumina ceramic armor are described. Fracture surfaces were examined by scanning electron microscopy, augmenting previous replication electron fractography studies. Direct transmission electron microscopy was employed in characterizing defect structures in extracted fracture fragments on replicas and in thin foils taken from bulk polycrystalline alumina in undamaged and damaged states.

A variety of dislocation interactions and tangled masses of dislocations with densities as high as 2×10^{11} cm^{-2} have been observed near intersecting surfaces in thin fracture fragments. Similar deformation textures within the bulk have been observed in impact-damaged alumina for a distance of at least 20 μm beneath a fracture surface. Localized plastic flow is most prominently evidenced in the case of cracks which are intersecting at acute angles to create fracture fragments, and in worked zones abutting propagating cracks in more massive material. These observations strongly support the concept that portions of the high stresses concentrated at the tips of propagating cracks during an impact event are relaxed by plastic deformation processes, thereby absorbing excess energy and/or delaying the fracture process to some degree.

ACKNOWLEDGMENTS

Alumina ceramic armor specimens selectively damaged under controlled ballistic impact conditions were obtained from the United States Army Mechanics and Materials Center, Watertown, Massachusetts, through the cooperation of Dr. J. J. Burke and Capt. J. J. Stiglich, Jr.

Many faculty and staff members at North Carolina State University have participated in valuable discussions, technical assistance, and critical reviews in connection with this project. Our particular thanks are expressed to W. W. Austin, W. W. Kriegel, H. H. Stadelmaier, R. B. Benson, Jr., R. A. Douglas, P. F. Becher, and E. M. Gregory. M. L. Huckabee and C. E. Zimmer provided experimental assistance and contributed in the preparation of this report.

TABLE OF CONTENTS

LIST OF TABLES

LIST OF FIGURES

LIST OF FIGURES (continued)

LIST OF FIGURES (continued)

INTRODUCTION

Although fine details of possible fracture processes in ceramic oxides are not yet adequately known, many efforts have been made to obtain a better understanding of the basic fracture mechanisms. The functional dependence of fracture strength on microstructural parameters has been only partially developed in these oxide ceramics. Study of the fracture behavior of polycrystalline ceramics depends on a detailed insight into the mechanisms of the formation and propagation of cracks in these materials. The nature and distribution of grains and phases in a material, the role of grain boundaries and substructures, their intrinsic strengths, and externally applied stresses and strains are important considerations in this approach. In addition, the anisotropic nature of most ceramic crystals and the inability of individual crystals to change shape freely when confined in a polycrystalline body contribute further to highly localized states of stress and strain. These factors generally give rise to very complex fracture behavior and quite often may lead to strength anomalies. These topics in physical ceramics have been considered from several viewpoints and in considerable detail in reviews by Kingery and Coble (1963), Stokes (1964), Palmour (1964) and Davidge (1969).

The Griffith crack theory (Griffith, 1920), dealt with brittle fracture from the point of view of the flaw theory of solids, in which fracture is predicated upon the presence and propagation of pre-existing flaws in a critically stressed solid. However, fracture surface energies for α-Al_2O_3 abnormally higher than the surface free energy calculated from chemical considerations have been observed by many investigators

(Congleton and Petch, 1966; Gutshall *et al.*, 1967; Swanson and Gross, 1968; and Wiederhorn, 1969). Such discrepancies between measured fracture surface energies and normal chemical surface energies in the case of nominally brittle ceramics strongly suggest that one should consider, and investigate experimentally, the possibility of additional energy absorption akin to plastic work energy (Orowan, 1948) in the intense stress fields which exist under conditions of quasi-hydrostatic restraint at and near the tips of propagating cracks during impact events (Palmour *et al.*, 1969).

The objectives of the present research were to examine microstructural features, including fractographic textures and defect substructures, in a typical commercially produced polycrystalline alumina subjected to fracture by ballistic impact, and to establish their relationships to energy absorption processes occurring during impact fracture. The over-all study program was divided into three areas, *i.e.*, (1) optical and electron optical fractography studies of sheared, spalled, and cracked α-Al_2O_3 single crystal and ceramic surfaces produced by ballistic impact events, (2) thermoanalytical measurements of thermally activated releases of shock-induced internal strain energy, and (3) direct examinations of dislocations and other structural defects in impact produced fragments and bulk material by transmission electron microscopy, coupled with direct examination of ballistic fracture surfaces by scanning electron microscopy. Results obtained in parts (1) and (2) have been reported in detail elsewhere (Palmour *et al.*, 1969). The work presented here, drawn from the third phase, seeks to obtain better insights on a fine microstructural scale of those fracture

mechanisms which actually occur in oxide ceramics under ballistic impact conditions.

REVIEW OF LITERATURE

Mechanics of Ballistic Penetration of Ceramic Armor

The introduction of ceramics to armor design brought about a considerable amount of study concerning the mechanics of penetration, energy transfer and absorption after the armor had begun to crack, and projectile-armor interaction. The following section, which is based largely on the text by Martin (1969), describes some of the prevalent views on the ballistic penetration mechanics of composite ceramic armor.

Three major structures are involved in the composite ceramic-armor problem: the ceramic, the backup material and the bullet. These three elements cannot be considered as independent since each is of major importance in the penetration event. Figure 1 is a schematic which shows the sequence of events in a penetration event. Upon impact, the hard steel bullet "splashes" on the ceramic until the plate completely fails, at which time the projectile begins to penetrate the broken ceramic. Pressure transmitted through the broken ceramic causes deformation in the backup plate. As the projectile penetrates the ceramic, the influence of the projectile on the backup becomes more and more local as the projectile approaches the backup. If the projectile has been decelerated enough early in the event, it will stop before penetrating the backup. The ceramic plate fails after some length of time and whatever is left of the projectile enters a new phase of penetration, that of penetrating the broken ceramic and deforming the backup plate. The length of time it takes the ceramic to fail is therefore of major importance.

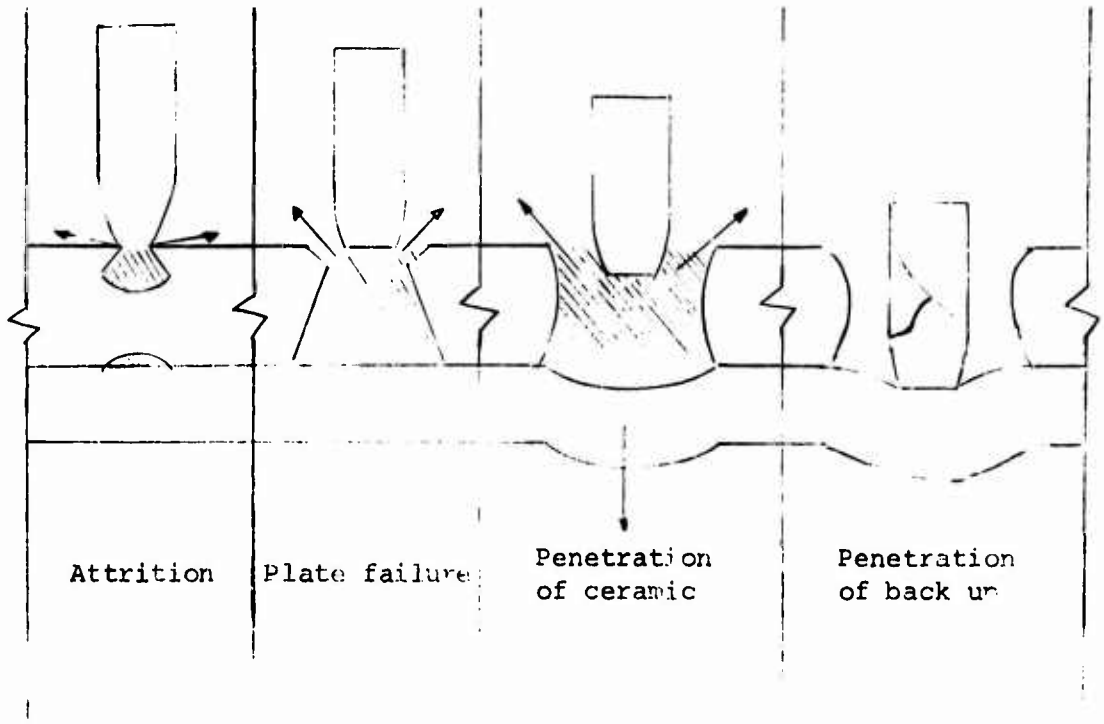

Figure 1. Schematic of penetration event (after Martin, 1969)

The thickness of the ceramic involved in the penetration event is intimately connected with the length of time to failure and to the distribution of force on the backup plate.

Fracture Produced by Stress Waves

The pertinent literature on fracture behavior in solids induced by explosive shockwaves has been reviewed in detail by Rinehart (1951), Kolsky (1953), and Kolsky and Rader (1968). Their papers provide the basis for the following discussion.

When a stress pulse of sufficiently large amplitude travels through a brittle solid, it may produce fracture phenomena which differ in several important respects from those produced under conditions of quasistatic or relatively slow dynamic loading. These are:

1. Any cracks that are formed for pulses of short duration do not have time to grow before the pulse has passed.
2. A localized region of the specimen is stressed.
3. When a compressive pulse is incident on a free boundary, it gives rise to a reflected tensional pulse.

When a bullet impinges on a large sheet of material, or when an explosive charge is detonated in contact with it, a high spherical compressional pulse of very short duration is sent into the material. When this pulse arrives at the bottom face of the specimen, it is reflected as a pulse of tension. This reflected tensional pulse will pass through the tail of the incident compression pulse so that the resultant stress in the plate will be the sum of the stresses due to the incident and reflected pulses.

Fracture will begin at the region where appreciable tensile stress will be first set up, which is some distance from the free surface. Once a fracture has started, the rest of the pulse is reflected at the new free surface formed, so that a series of parallel cracks may be produced when the amplitude of the stress pulse is sufficiently great.

Plastic Deformation in Crystalline Ceramic Solids

Ceramics are classically considered to be brittle materials because they appear to be incapable of plastic deformation. During recent years, the realization has gradually developed that certain ceramic crystals are not truly brittle at normal temperatures. Many investigators (Nye, 1949; Gilman *et al.*, 1958a; Gorum *et al.*, 1958; Johnston and Gilman, 1959; Parker, 1961) have demonstrated that crystalline ceramics, under suitable circumstances, exhibit plastic properties like those normally

associated with metals. Stokes (1964) pointed out that plastic deformation in a crystalline ceramic at low temperature (*i.e.*, < 0.5 T_m) is due to the generation, motion, and multiplication of dislocations, and noted that the combined influences of bond character and crystal structure have their greatest effect on the relative mobility of dislocations in various ceramic materials. When a dislocation moves, ionic and covalent bonds must be broken and remade, and in the case of a dissociated dislocation, the partials must also be moved along together. Only at high temperatures (> 900° C, where ion mobility is high) can dislocations be made to move easily in alumina. On the other hand, the predominantly ionic nature of the bond and the relative simplicity of the dislocation configuration in MgO makes it possible to deform this material even at liquid nitrogen temperatures.

The alternative to plastic flow is stress buildup and eventual fracture, and it is clearly enhanced by high strain rates, high stress levels, relatively more difficult transport processes, and low temperatures (Palmour, 1964). If the strain rate becomes so high that neither the number of available dislocations nor the critical velocity can keep up, then the stress will rapidly increase until it reaches a level at which catastrophic failure will occur. Even if propagatable cracks are not initially present, dislocation pile-ups and interactions can create them. Stroh (1955) has proposed such a mechanism of crack initiation by dislocation pile-up and coalescence and Stokes *et al.* (1958) have observed Stroh-type cracks in deformed MgO single crystals.

In his review, Palmour (1964) noted that the pile-up of dislocations in single crystals occurs chiefly at the surface or at intersections of slip bands, but in polycrystalline material, grain boundaries offer the

principal obstacle to dislocation passage. It was pointed out that for plastic deformation to occur in polycrystalline materials, each individual grain must be able to undergo a generalized change in shape, and in addition sliding at grain boundaries must also take place. If the grains cannot change their shapes, some grain boundary sliding will occur, but as the level of strain increases, voids or cracks will have to develop, particularly at grain boundary nodes.

Additional detailed information on the subject of plastic deformation in ceramic materials will be found elsewhere (Johnston *et al.*, 1962; Stokes, 1964; Palmour, 1964; Congleton *et al.*, 1968; Heuer *et al.*, 1970; Becher, 1970).

Energy Dissipation During Cleavage Fracture

Cleavage steps, river patterns and hackles are commonly observed in the fracture surface of brittle or semi-brittle crystalline solids. Low (1959) commented that for a cleavage step to form, additional energy is required, and the propagation of the cleavage crack is therefore made more difficult. Thus, in addition to the surface energy and kinetic energy which must be supplied to propagate the crack, an additional amount of energy, some of which has been absorbed in the formation of cleavage steps, must be supplied by the available elastic strain energy if the crack is to continue to propagate. He also noted that the most common cause of cleavage step formation is the presence of screw dislocations that cut the cleavage plane. The screw dislocation responsible for cleavage steps may have been introduced into the crystal in two ways:

1. Grown-in dislocations present in any real crystal (Low, 1956; Gilman, 1958).
2. Dislocation induced by plastic deformation, either by deformation of the whole crystal before cleavage occurs (Gilman *et al.*, 1958b) or by glide at or near the tip of the moving cleavage crack.

Gilman *et al.* (1958b) has pointed out that the latter case arises only if the crack velocity is low enough or if the temperature at which this cleavage occurs is high enough.

The cleavage fracture of a randomly oriented polycrystalline aggregate is extremely complex compared with the cleavage fractures of single crystals. Gilman (1956) pointed out that if the misorientation of the cleavage plane in the next grain is small, then the crack front can cross the boundary with no change except for the appearance of large cleavage steps originating at the boundary. If the misorientation is large, the crack will have to propagate discontinuously by starting a new crack in the succeeding crystal. In either case there will be a sudden change in the energy absorption as the crack crosses the boundary.

Fractography

The very small depth of field (~ 0.2 microns) of the optical microscope makes photomicrography of the nonplanar surfaces almost impossible. The electron microscope with a relatively larger depth of field, much higher resolving power and a large range of magnifications is an ideal tool to study deformed and fractured surfaces. A complete evaluation of the fracture paths and fracture features requires a basic knowledge of the different mechanisms of fracture and also some meaningful

information on the nature and microstructure of the specific material. Detailed electron fractographic studies of ballistically damaged alumina ceramics and their interpretations have been described elsewhere (Palmour *et al.*, 1969), from which the following summary has been drawn.

Though electron fractography provides a powerful means for the study of fracture surfaces when compared to optical microscopy, the replication technique with its several limitations allows at best only an indirect examination of the fracture surfaces. The preparation of a shadowed replica of a fracture surface usually involves a one-, two-, or three-step process. These processes are usually very time-consuming and require great skill. Even then, the surface topography is not explored at all or, at best, is explored indirectly by the varying density of shading on the replica shown as bright and dark areas on the final two-dimensional images. In addition, spurious structures or "artifacts" attributable to replication itself (and hence not associated with fracture phenomena) are often produced. Thus, replication electron fractography requires great care and skill in preparing, handling, examining, and interpreting the fractographs.

In contrast, the scanning electron microscope offers a new approach to the analysis of fracture surfaces. This technique provides for the direct examination of surfaces with a depth of focus (for comparable magnification) nearly 300 times greater than optical microscopes, with a resolution approaching 200 Å. Also relatively large areas of the samples can be studied at one time (at as low as 60 to 100 diameters) to present a better picture of the over-all fracture phenomena, as compared to replicas where very small areas have to be carefully selected for study (at magnifications typically greater than 3000 diameters).

The scanning electron microscope differs radically from the transmission electron microscope by producing a magnified image through scanning, *i.e.*, without any lenses interposed between the specimen and the screen upon which the image is displayed. Details of scanning electron microscopy principles and techniques are given elsewhere (Thornton, 1968; Johari, 1968, 1969).

Transmission Electron Microscopy for Direct Imaging of Crystalline Defects

Electron contrast theories relating to imaging of crystalline defects have been reviewed in detail by Hirsch *et. al.* (1965), Smallman and Ashbee (1966), and Patterson and Wilsdorf (1968). These are the principal texts from which the following summary has been developed.

When an electron beam strikes a suitably oriented thin crystalline foil, there emerges from the other side two beams, one strongly diffracted and the other strongly transmitted. If the incident beam passes through a crystal lattice near a defect, *e.g.*, a dislocation, it encounters a localized change in diffraction conditions and the diffracted, and hence the transmitted, intensities are correspondingly modified. As a result, the defect can be distinguished from the background, *i.e.*, it shows diffraction contrast. On a bright-field micrograph, structural anomalies such as dislocations which strongly diffract electrons appear dark on a bright background since the transmitted intensity from these regions is less than that from the surrounding perfect crystal. For a dark-field image, this contrast is reversed. In order to explain the contrast observed at lattice defects, it is necessary to calculate the diffracted intensity from a perfect crystal and then try to see how this intensity is modified by the presence of lattice defects.

A dynamical theory taking account of the equilibrium between all waves in the defect crystal is required to describe completely the diffraction contrast from lattice defects. However, a simpler kinematical theory has been developed by Howie and Whelan (1961, 1962). Although it is an approximation justified only when the deviation from the reflecting position is large or when the crystal is very thin, this theory explains many contrast effects.

EXPERIMENTAL PROCEDURE

Two ballistically damaged polycrystalline alumina ceramic tiles obtained from other investigators[1] were subjected to detailed examination in this study. They originally measured 6 inches × 6 inches × 0.30 inch and had 5 pounds/sq ft areal density. Typical properties of standard Coors AD-94 polycrystalline alumina (~ 94 percent α-Al_2O_3), of which the ceramic armor tiles used in this study were composed, are listed in Table 1.[2] Nearly identical ceramic materials used in earlier electron fractography and thermoanalytical studies were described in a previous work (Palmour *et al.*, 1969).

Table 1. Typical properties of Coors alumina ceramics

Property	Test method	AD-94
Specific gravity	ASTM C-20-40	3.62 g/cm^3
Flexural strength	ASTM C-369-66T	51,000 psi
Compressive strength	ASTM C-528-63T	300 × 10^3 psi
Tensile strength		27,000 psi
Modulus of elasticity	Sonic method	41 × 10^6 psi
Shear modulus	Sonic method	17 × 10^6 psi
Bulk modulus	Sonic method	24 × 10^6 psi
Poisson's ratio	Sonic method	0.21
Sonic velocity	Sonic method	8.9 × 10^3 m/sec
Hardness	ASTM E-18-66	78 (Rockwell 45N)

[1]Specimens provided by Captain J. J. Stiglich, Jr., Ceramics Laboratory, United States Army Mechanics and Materials Research Center, Watertown, Massachusetts, October 6, 1969.

[2]Data from Coors Alumina and Beryllia Properties Handbook, Coors Procelain Company, Golden, Colorado.

The specimens selected had been impacted by a 0.30 caliber ball (lead alloy) projectile at 2266 feet per second (Tile 1), and a 0.30 caliber APM-2 armor piercing projectile at 2224 feet per second (Tile 7), respectively.[3] One corner had been removed from each tile prior to impact to serve as an unshocked control. For the test shots, these tiles had been cemented to and were supported by 12 inch × 12 inch × 1/4 inch glass reinforced plastic backing material. Different damage patterns related to projectile types are evident in the macroviews of Figure 2. The softer lead alloy ball projectile gives a broader, more disperse fragmentation pattern, while the armor piercing projectile produced a more concentrated and more intense fragmentation over a relatively smaller area.

All available fractured fragments were reassembled into the original configuration. Macroscopic views of these ballistically damaged polycrystalline alumina tiles are shown in Figure 2. Interior views of these tiles after removal of frontal spall fragments are shown in Figure 3.

Thinning Ceramic Foils for Transmission Electron Microscopy

Preparation of a selected fracture fragment for transmission electron microscopy was accomplished with a combination of mechanical polishing and ion beam thinning. Detailed procedures for thinning of ceramic foils by ion beam bombardment have been described elsewhere (Tighe, 1970; Becher, 1970).

---

[3]The composite armor (tile, cement, and backing) successfully defeated each of the projectiles at the test velocity.

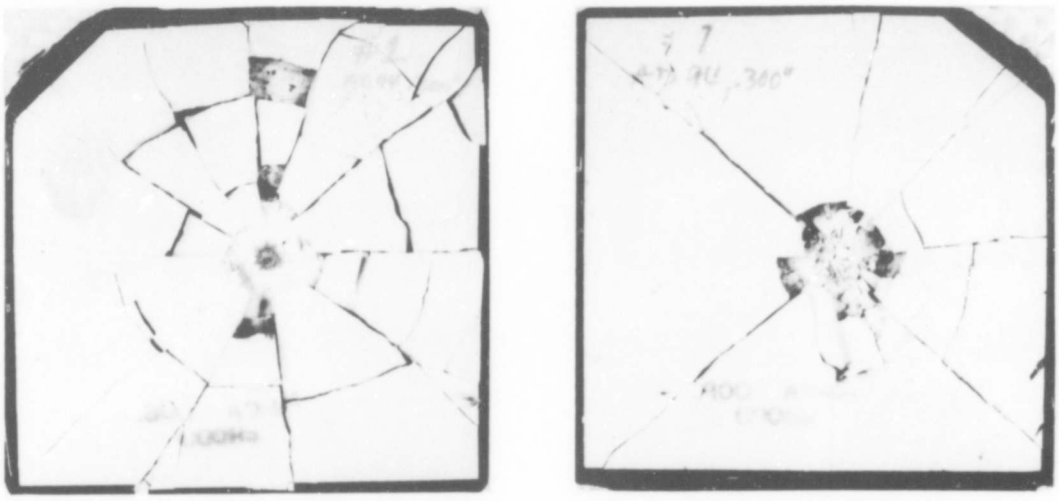

(a) (b)

Figure 2. Macroscopic damage in alumina armor tiles caused by ballistic impact with different projectiles at 2240 feet per second: (a) 0.30 caliber ball (lead alloy); (b) 0.30 caliber APM-2 armor piercing (reassembled front faces of 6 inch × 6 inch × 0.30 inch alumina ceramic tile 1 (a) and tile 7 (b); corner had been removed from each tile prior to impact to serve as unshocked control)

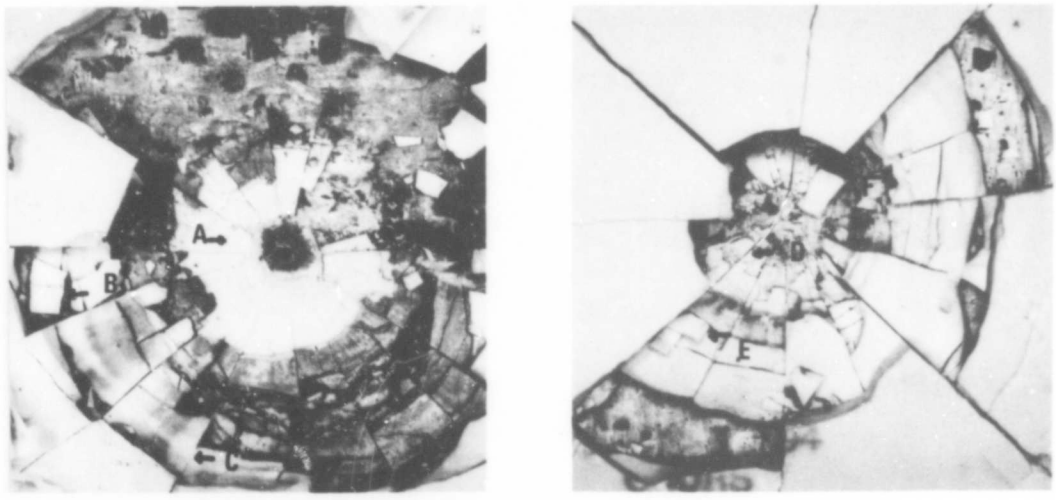

(a) (b)

Figure 3. Interior views of 6 inch × 6 inch × 0.30 inch alumina ceramic tile 1 (a) and tile 7 (b) after removal of frontal spall fragments (arrows and letters indicate chips sampled for transmission electron microscopy studies)

Disk shaped samples of microscope grid size (~ 3 mm diameter) were cut from the fracture fragments using an ultrasonic instrument[4], and then were ground to 10 mil thickness. Thereafter, these disks were mechanically polished to 1-3 mil thickness on an automatic polishing machine[5] employing hard maple laps impregnated with 30, 14, and 6 micron diamond paste with filtered kerosene lubricant. In some samples it was not possible to polish to less than 4 mils as the disks fractured due to impact induced cracks. For such materials, an alternate procedure was employed in which a depression (dimple) was made in the surface of 10 mil thick disks using the ultrasonic machining apparatus, yielding a thicker outer ring to support the thinned central region. The prepared disk was then placed in the sample holder of the ion beam thinning device[6] and exposed *in vacuo* to two multibeam ion sources which impinge from opposite sides of the inclined, rotating specimen stage. Argon served as the ionizable gas; it is ionized and accelerated toward the sample under operating voltages of 5 to 6 kv and currents of 1.0 to 1.2 ma. The sample surface is in effect eroded under the bombarding action of inert gas ions, with thinning rates of up to 2 μm/hr being commonly achieved with these alumina samples.

After the sample was adequately thinned, denoted by development of one or more holes, one surface of the sample was coated *in vacuo* with

---

[4]Cavitron Ultrasonic Machine Tool, Model 200B, Sheffield Company, Dayton, Ohio.

[5]UNI-POL, Model UPC-1, Geoscience Instrument Corp., New York, New York.

[6]Ion Micro Milling Instrument, Model IMMI-2, Commonwealth Scientific Corp., Alexandria, Virginia.

a carbon film (to prevent surface charging during irradiation in the electron microscope) and then inserted in a folded copper microscope grid.

Thinning rate is effected not only by the operating voltage and currents but also by the angle of tilt between the ion beam and sample surface. Generally tilt angles of 15° to 20° were employed with the result that second phases were retained and thinning was uniform from grain to grain.

Transmission Electron Microscopy

Fracture fragments retained on two-stage carbon replicas which had been prepared for electron fractography studies in previous work (Palmour *et al.*, 1969) and various thinned foils prepared by the technique described in the foregoing section were examined in a transmission electron microscope[7] using an accelerating potential of 120 kv. Two specimen stages were used in this study, each capable of 360° rotations but limited to tilts of 8° in one case[8] and 30° in the other[9]. The techniques which were used to observe defects and other microstructural characteristics are essentially those described in the text by Hirsch *et al.* (1965) as well as those employed by Tighe and Hyman (1968), Tighe (1970), Heuer *et al.* (1970) and Becher (1970).

---

[7]Model JEM 120, a product of Japan Electron Optics Laboratory Company, Ltd., Tokyo, Japan.

[8]Model JEM-AIG-212, a product of Japan Electron Optics Laboratory Company, Ltd., Tokyo, Japan.

[9]Model JEM-AIG-1, a product of Japan Electron Optics Laboratory Company, Ltd., Tokyo, Japan.

Interpretation of Electron Diffraction Patterns

Detailed procedures for indexing of electron diffraction patterns and identification of Burgers vectors in aluminum oxide were described in a recent dissertation (Becher, 1970), from which the following summary has been drawn.

The Burgers vectors of the various dislocations analyzed were determined using the techniques described by Hirsch *et al.* (1965). Briefly, the basic method involved obtaining diffraction contrast conditions (from a selected small area including the defect in question) that resulted in the observed dislocation being either in or out of contrast by employing a strongly diffracted beam, *i.e.*, a two-beam case. Generally two or three different out-of-contrast conditions were required to unambiguously identify the type of dislocation involved. By employing a strongly diffracted beam, the reciprocal space vector, $\bar{g}$, representing the diffraction plane could be identified from the diffraction pattern. When the $\bar{g}$'s of the in- and various out-of-contrast conditions were obtained, they were then employed in the following equations:

$$\bar{g}_{hkl} \cdot \bar{b} = 0 \qquad \text{dislocation out of contrast}$$

$$\bar{g}_{hkl} \cdot \bar{b} \neq 0 \qquad \text{dislocation in contrast}$$

where $\bar{b}$ was necessarily the Burgers vector of a screw dislocation of the above conditions to be strictly applied. For alumina, dislocations can have Burgers vectors of $\langle 11\bar{2}0 \rangle$ and $\langle 10\bar{1}1 \rangle$ or possibly $\langle 10\bar{1}0 \rangle$. These Miller-Bravais indices must be converted to Miller indices prior to doing the vector dot-product operation:

$$\bar{g}_{hkl} \cdot \bar{b} = (hlk) \cdot [uvw] \quad .$$

Valid solutions were obtained employing all possible Burgers vectors in the dot-product equation and determining which corresponded with observed contrast conditions.

Scanning Electron Microscopy

To obtain intact fracture surface topography, scanning electron microscopy was used by taking advantage of higher resolution and large depth of focus compared to light (optical) microscopy.

Fracture debris or dust was carefully removed from fracture fragments taken from various areas selected for detailed analysis. Thereafter the sample was cemented, fracture surface up, to a cylindrical brass specimen holder (3/8 inch diameter by 3/8 inch high), then the surface was omnidirectionally coated *in vacuo* with a thin conductive metallic layer (usually a gold-palladium alloy, occasionally pure gold).

The prepared samples were then examined in the scanning electron microscope[10] using an accelerating voltage of 25 kv. All of these studies were carried out under the same basic operating conditions, except that the fracture surfaces had various tilt angles (0° to 45°) with respect to the beam. Micrographs (secondary electron images) of various samples were photographed at appropriate magnifications (up to 20,000 diameters), using Polaroid P/N-55 film.

---

[10]Model JSM-2, a product of Japan Electron Optics Laboratory Company, Ltd., Tokyo, Japan.

RESULTS

Replication Fractography

Replicas of ballistically damaged alumina fracture surfaces examined at high magnifications with the electron microscope have provided numerous examples (and significant structural details) of localized plasticity associated with impact fracture. Detailed procedures for electron fractography and interpretations of fractographs taken from ballistically fractured single sapphire and polycrystalline alumina ceramics have been described elsewhere (Palmour *et al.*, 1969). One representative electron fractograph of polycrystalline alumina (Kim, 1969) is reproduced in Figure 4. The micrograph shows several interesting examples of interaction between the advancing crack and the crystalline substructure (principally subgrain boundaries). These interactions apparently result in very local alterations of the fracture texture. Multiplications and redirections occur at the grain boundary marked by line A - A'; other changes along B - B', C - C', D - D', D' - D", and B' - D' may be indicative of the influence of subgrain boundaries. Arrows in the micrograph indicate local directions of the advancing crack.

Evidences of Fracture Induced Plastic Deformation

Two-stage plastic replicas taken from ballistically damaged alumina fracture surfaces, initially prepared and examined in electron fractography studies in previous work (Palmour *et al.*, 1969) contained many fracture fragments. Some of them were thin enough to permit reasonably effective study of internal defects by direct transmission electron microscopy at an accelerating potential of 120 kv.

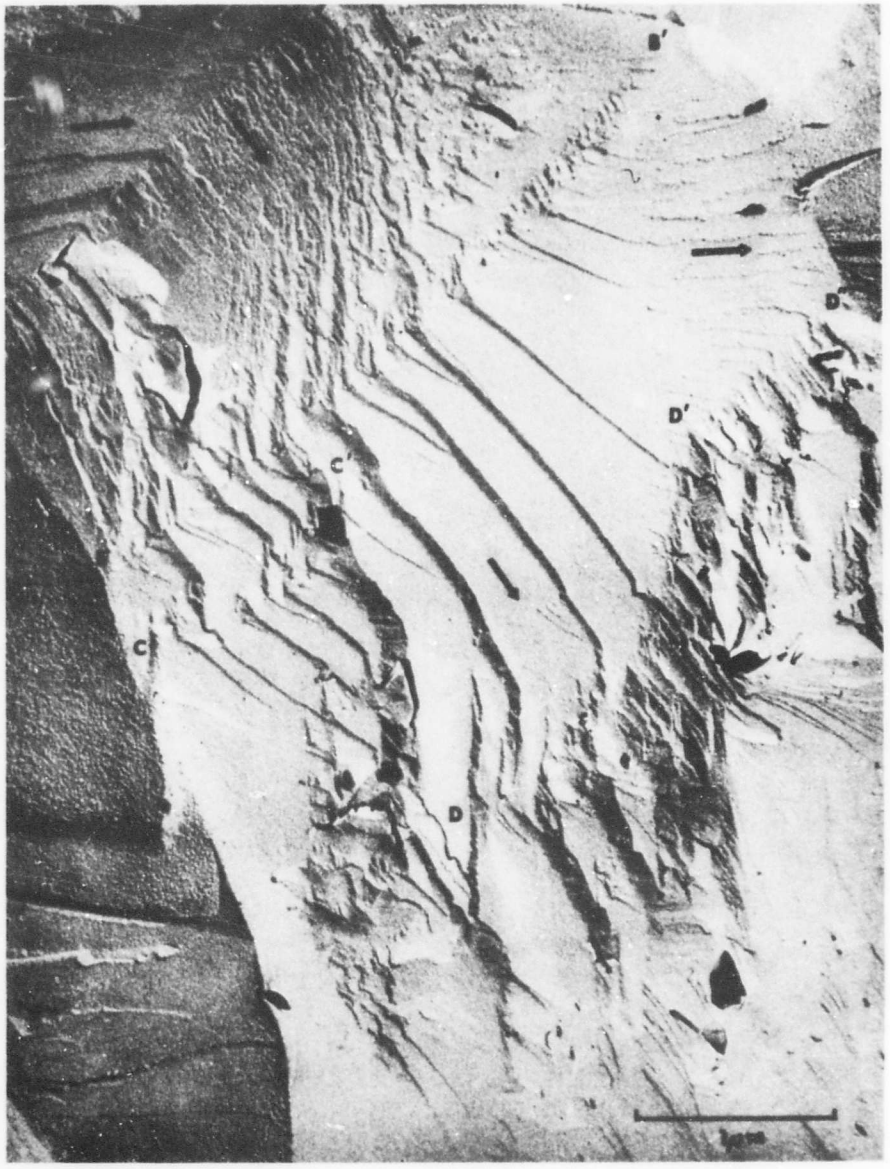

Figure 4. River pattern cleavage steps on a transverse secondary crack in ballistically damaged polycrystalline alumina tile; two-stage plastic-carbon replica, Pt-shadowed at 30° (after Kim, 1969)

Results obtained from study of such fragments derived from various fracture regions (produced by an impacting armor piercing projectile in 94 percent alumina) are described in the following sections.

Fragments from Conoid Shear Surface

Heavy concentrations of dislocations were found in detailed examinations of one such fragment from the conoid shear surface, and though Burgers vectors were not specifically identified, contrast effects suggested that several sets of disolocations were involved. This prior work was described in detail by Palmour *et al.* (1969).

Fragments from Smooth Radial Crack Surface

The micrograph in Figure 5a represents diffraction contast associated with defects (dislocations) in a transparent fracture fragment extracted from a relatively smooth portion of the radial crack surface. Of particular interest in the micrograph are the dislocation configurations in regions marked A, B, and C. Individual dislocations are evident within region B. Such dislocations are also present in area A, shown in greater detail at somewhat higher magnification in Figure 5b. In region C, the density of defects was too great to permit resolution of individual dislocations. Similar dislocation densities associated with the region of contact between a sapphire crystal and a diamond indenter was reported by Hockey (1970). Such dislocation entanglements at or near the edges of chips were commonly observed throughout this transmission electron microscopic study of ballistically produced fracture fragments. Similar findings have been reported by Congleton *et al.*, 1968, 1969) for alumina fragments resulting from single stroke fracture at much lower nominal strain rates.

Local dislocation density in region A (Figure 5b) has been estimated to be at least $2 \times 10^{11}/cm^2$. This value is approximately 6 orders of magnitude larger than those reported for grown-in dislocations in sapphire by Scheuplein and Gibbs (1960). By tilting the fragment to obtain a variety of two-beam diffraction conditions, the Burgers vector of these dislocations has been determined to be of $\langle 1\bar{1}01 \rangle$ type according to the invisibility criterion $g \cdot b = 0$.

Though detailed evaluation has not always been available due to poor diffraction conditions in thick regions, a considerable degree of complexity of dislocation entanglement has been observed in other transparent fracture fragments (Figures 5c and 5d) from the same region of this radial crack surface. Regions marked D and E in Figures 5c and 5d, respectively, show dislocations arrayed in a variety of slip traces and interactions, providing direct evidence for dislocation movement associated with generation of the fracture chip. Obviously, the high stresses concentrated at the tips of cracks propagating during impact (specifically, those creating the fragment) have been relaxed to some degree by such deformation processes. This view is consistent with Friedel's (1959) conclusion that plastic relaxation can occur by making neighboring dislocations move or even by creating new ones in regions near a propagating crack tip.

Fragment from Rough Radial Crack Surfaces

The later portions of the primary radial cracks are composed of very rough surfaces with complex textures. Figure 6 shows diffraction contrast micrographs of an extracted transparent fragment on a replica from such a rough surface.

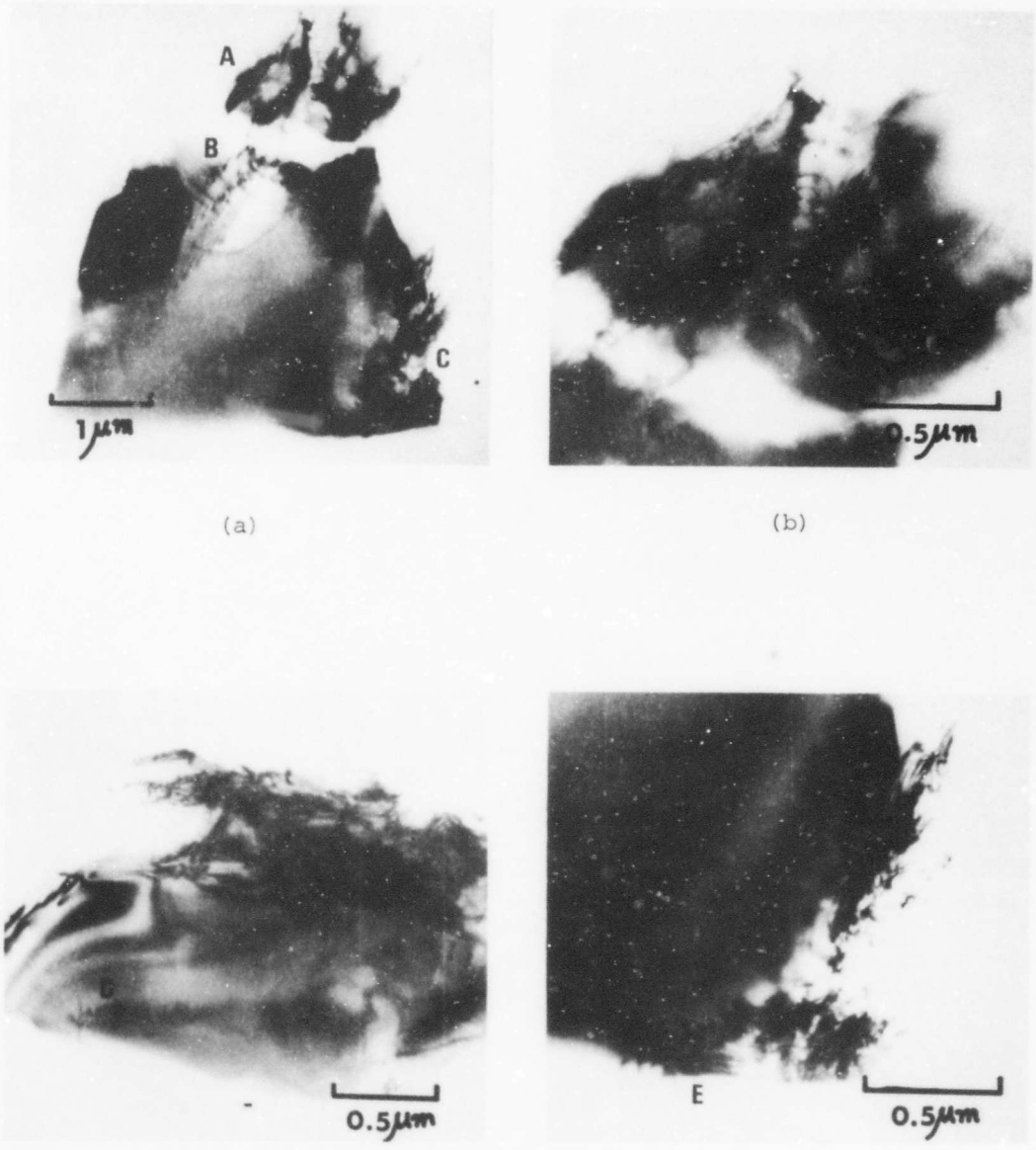

Figure 5. Structural defects in extracted fracture fragments from smooth radial surface in ballistically damaged polycrystalline alumina tile (letters locate dislocations and other features described in text): (a) diffraction contrast micrograph associated with defects in the regions marked A, B, and C; (b) higher magnification micrograph of the region marked A in Figure 5a; (c) dislocation arrays in the region marked D; (d) dislocation arrays and interactions in the region marked E

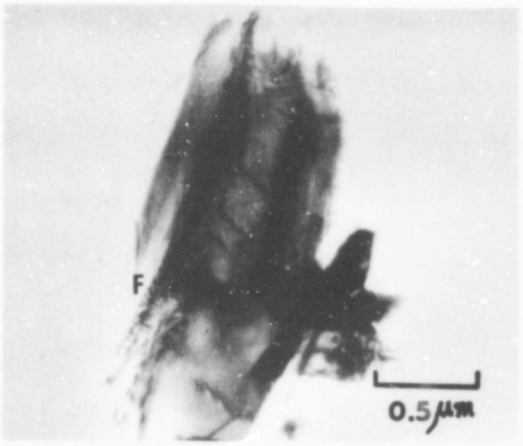

(a)

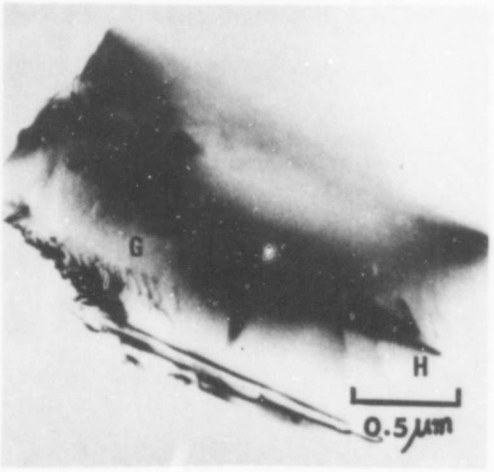

(b)

(c)

Figure 6. Structural defects in extracted fracture fragments from a rough radial crack surface in ballistically damaged polycrystalline alumina tile (letters locate dislocations and other features): (a) high density dislocation arrays and interactions in the region marked F; (b) dislocation arrays in the regions marked G and H; (c) heavy concentration of dislocations in the region marked J

As in the preceding examples, it can be seen that high density dislocation arrays were present in the fragment, providing *prima facie* evidence of plastic deformation processes. Selected area diffraction analysis revealed the Burgers vector of the dislocations (marked F) in Figure 6a is of the $<11\bar{2}0>$ type and that of those (marked G) in Figure 6b is of the $<01\bar{1}1>$ type.

Since dislocation pile-ups (aggregations) can occur only as a result of plastic deformation, these observations strongly suggest that crack propagation during impact fracture is accompanied by intense but local plastic deformation. Localized plastic flow seems particularly evident in the case of the intersecting cracks which created these fragments. Gilman (1958) reported that in LiF, dislocation nucleation accompanies the propagation of the crack tip, and also noted that when an advancing crack cuts through such a crack-nucleated dislocation loop or grown-in dislocations, cleavage steps are left behind. Somewhat similar effects have been observed in ballistically damaged alumina and are discussed in a subsequent section.

Defect Structures in Damaged Alumina Bulk

To supplement the study of structural defects in impact induced fracture fragments (possible only in those retained fragments thin enough to transmit electrons), direct transmission electron microscopy was employed also in the examination of foils deliberately prepared from bulk stock by ion bombardment. The latter specimens have been taken from much larger fragments collected from ballistically damaged tiles. They are representative of two areas: (1) in the immediate vicinity of the projectile-target impact point, and (2) at some distance from the

impact point (see Figure 3), particularly where reinforcements of reflecting waves produced heavy damage.

Control: As-Received Microstructure

One corner of each polycrystalline alumina tile was cut off and reserved as a control before the ballistic shot was performed, permitting investigation of the microstructure in the undisturbed condition.

Microstructural examination of the control sample revealed that pre-existing dislocations were generally in two forms. One form consisted of predominantly tilt sub-boundaries, occasionally with some of twist character (Figure 7). The other form consisted of dislocation arrays associated with pores within grains, or in limited instances, of individual dislocations within grains. Beside the alumina grains, a substantial amount of glassy phase was distributed between grains, mainly in triple points. Foreign phases were also observed, mostly in triple junctions.

Defect Structures in Alumina Tile 1 After Ballistic Damage

Dislocation arrays in the form of small-angle boundaries or sub-boundaries (most of tilt character, some with twist character) were often seen. However, such boundaries composed of dislocations occasionally revealed complex fringe patterns. The dislocations forming the sub-boundaries can be revealed after tilting the specimen with respect to the electron beam to obtain different diffraction conditions. Grain boundaries with high angle misfit can be imaged as a set of equal thickness fringes or as lines, depending on the orientation of the boundary with respect to the electron beam and on the operating reflection plane. One good example of an extensive dislocation network forming sub-boundaries is illustrated in Figure 8.

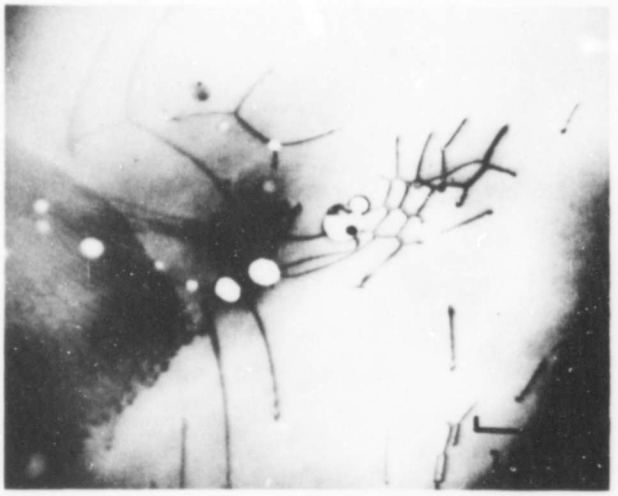

Figure 7. Dislocation configurations of unshocked control (corner, tile 1, Figure 2a)

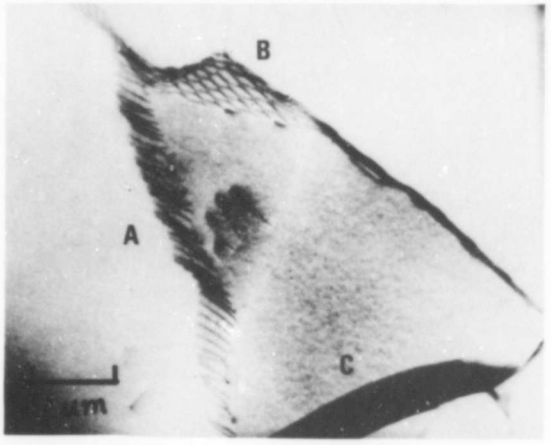

Figure 8. Typical microstructural features in ballistically damaged polycrystalline alumina showing tilt and twist boundaries, and high angle boundary fringe contrast (tile 1, chip A, Figure 3a)

The boundary marked A is a tilt wall, with the dislocations inclined to the foil. The interaction of a single dislocation with this tilt wall making an array of nodes is also seen. A dislocation network forming a simple twist boundary is shown at B. A grain boundary fringe contrast resulting from an interface inclined to the electron beam is noted at C. Figure 9 illustrates an inclined boundary of nearly pure tilt character which interacted with several single dislocations (left) and shows a moire fringe pattern resulting from complex fringe diffraction effects (right).

Since only a minute volume element can be sampled in a single foil, and the complexity of the techniques and the time required for analysis greatly restricts the number of foils which can be examined, it is not possible to describe rigorously, or even statistically, all of the dislocation structures pre-existing in the control material, or those additional ones corresponding to a given shock impact. At best, one must be content with qualitative, not quantitative, representations of the events in question. Nevertheless, in this study, sub-boundaries composed of interacted dislocations, crossed grids of dislocations, complex fringe patterns or moire patterns have been much more frequently observed in damaged alumina than in control specimens.

Dislocations which appeared to be related to shear of grain boundaries described by Gleiter *et al.* (1968) were occasionally observed, but boundary offsets at triple points which also would have been expected to result from grain boundary sliding were not found. These experimental observations suggest that the copious glassy phase (estimated by the manufacturer at ~ 16 volume percent) associated with boundaries and especially with triple junctions of this 94 percent alumina might either

alter or obscure the displacement of triple points, making this commonly accepted evidence of sliding much less likely to be observed than in the deformed alumina bodies of higher purity investigated by Heuer *et al.* (1970) and Becher (1970).

Ishida and Brown (1967) reported that the electron images of grain boundary dislocations are sometimes different from those of dislocations lying within the grains, and that the contrast of dislocations lying along a grain boundary can be reversed by changing the diffraction conditions. Figure 10 shows a bright field micrograph where both dark and light dislocation images are visible simultaneously at the grain boundary. Tilting experiments using the invisibility criterion $g \cdot b = 0$ showed that the white dislocations lying parallel to grain boundary had the $\langle 01\bar{1}1 \rangle$ type Burgers vector, while the dark set of dislocations had a $\langle 11\bar{2}0 \rangle$ type Burgers vector. It is suggested that the dislocations under consideration are associated with grain boundary sliding, or alternatively, are mismatch dislocations associated with lattice strains in a relatively high angle, non-symmetrical grain boundary.

Tangled masses of dislocations comparable to those seen in extracted fragments from fracture surfaces (discussed earlier) were also observed in damaged material thinned from bulk. Heavily interacted dislocation structures at the edge of an isolated thin grain are shown in Figure 11a. Determinations of the Burgers vector and slip plane were not possible because the specimen thickness prevented adequate diffraction data from being obtained. However, it is evident that plastic deformation was caused by the propagation of a plastic shock wave or subsequently induced during the adjustment of the advancing crack at the barrier.

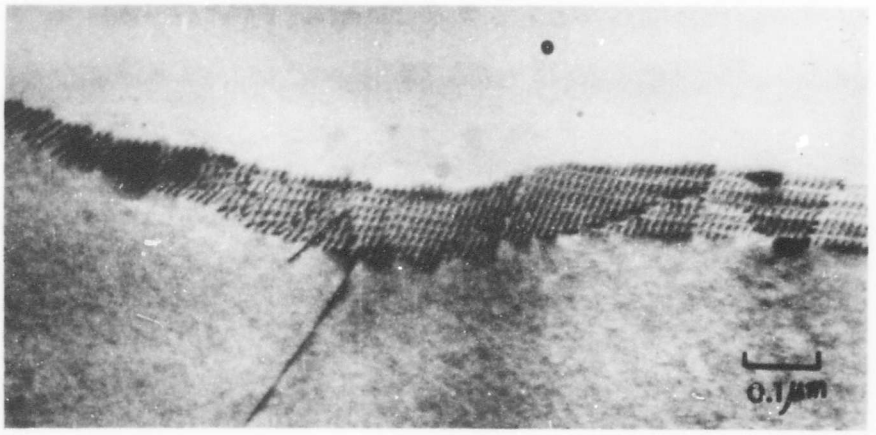

Figure 9. Typical microstructural features in ballistically damaged polycrystalline alumina showing inclined tilt boundary with foreign dislocations and a moire fringe pattern (tile 1, chip A, Figure 3a)

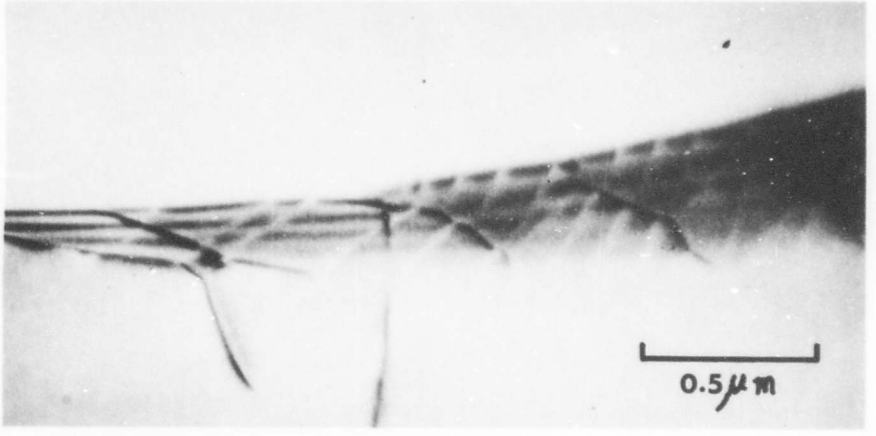

Figure 10. Typical microstructural features in ballistically damaged polycrystalline alumina: a bright field micrograph where both dark and light dislocation images are visible within the grain boundary (tile 1, chip C, Figure 3a)

The interaction of a group of dislocations adjacent to a transverse crack are shown in Figures 11b and 11c which have slightly different orientations with respect to each other. Extension of slip bands was halted in the interior of the grain possibly because of unseen barriers which lay above or below this very thin foil.

Loop-like or bowed-out dislocations between locking points were infrequently observed. An obstacle in the path of a glide dislocation, or a jog, resulting for example from the intersection of a gliding screw with another dislocation, can locally retard dislocation motion. Examples are shown in Figures 11d and 11e. The dislocations being held back and consequently being formed into loops by unseen point defects or jogs consisting of short segments of edge dislocations are visible in Figure 11d. Figure 11e demonstrates multiplication of dislocations by gliding dislocations at the unseen obstacle.

Substantial numbers of individual dislocations were seen in damaged material in this investigation. They were usually almost straight, of variable length depending upon their orientation with respect to the foil, and exhibited few features of interest (Figure 11f); however, one interesting feature is shown in Figure 11g. Here, dislocations crossed the unidentified obstacle and left the segment dislocations on the obstacle. Figure 12 shows dislocation structures attributed to impact damage generated by plastic shock waves. The low angle twist boundary at the top is of the type commonly observed in unshocked material, but other dislocations, especially the stepped arrays near the center, are not characteristic of the sintered alumina control, and may well have resulted from the impact event. They may have been formed by interaction of plastic shock waves with the pre-existing sub-boundary networks.

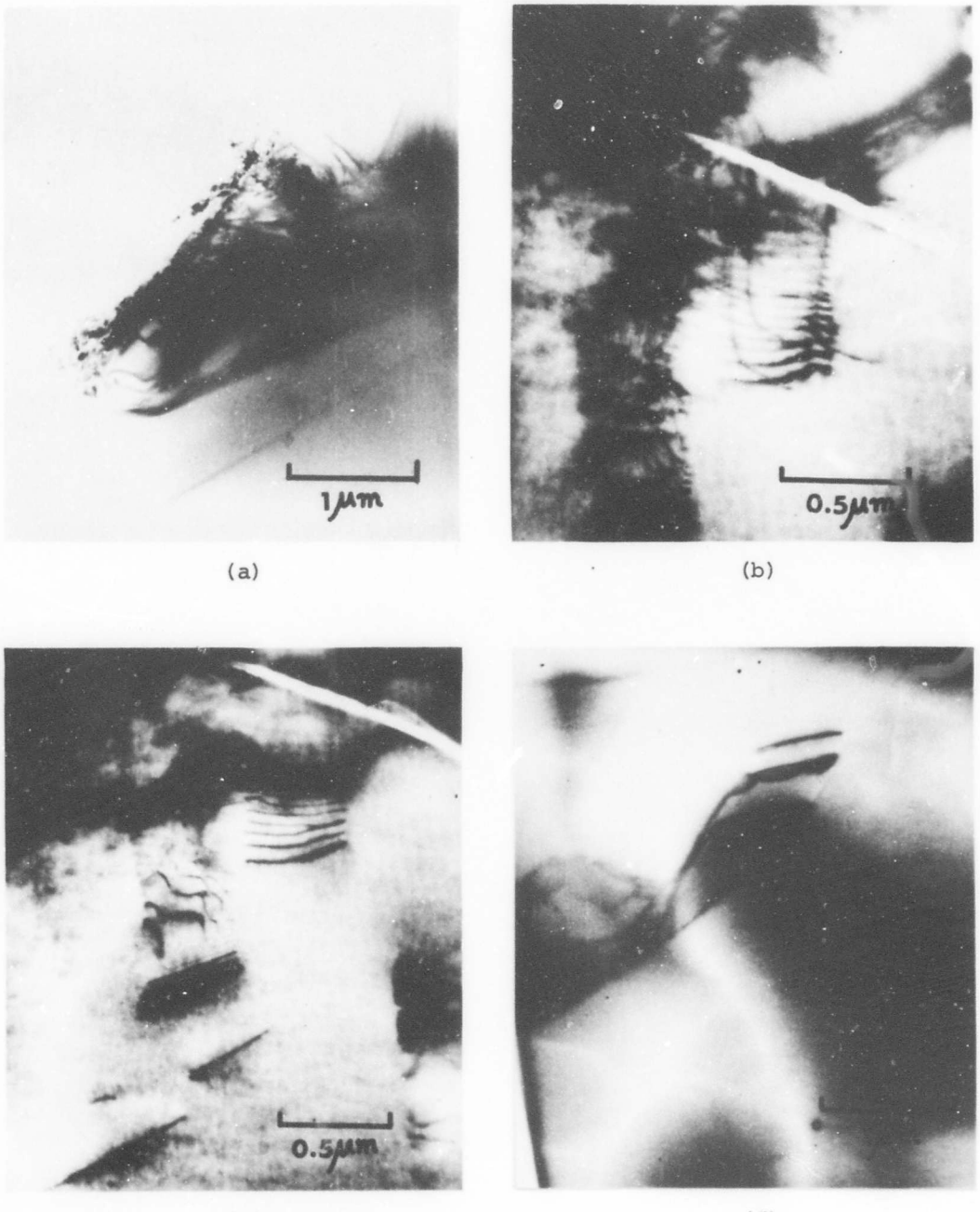

(a) (b)

(c) (d)

Figure 11. Dislocation structures associated with ballistic impact in polycrystalline alumina (tile 1, chip C, Figure 3a): (a) heavily interacted dislocation structures at the edge of an isolated thinned grain; (b) the extension of slip bands adjacent to a crack; (c) the same area as (b), tilted to slightly different orientation; (d) dislocation loops formed during glide; (e) bowed-out dislocations; (f) individual dislocations; (g) dislocation is segmented by an obstacle

(figure continued)

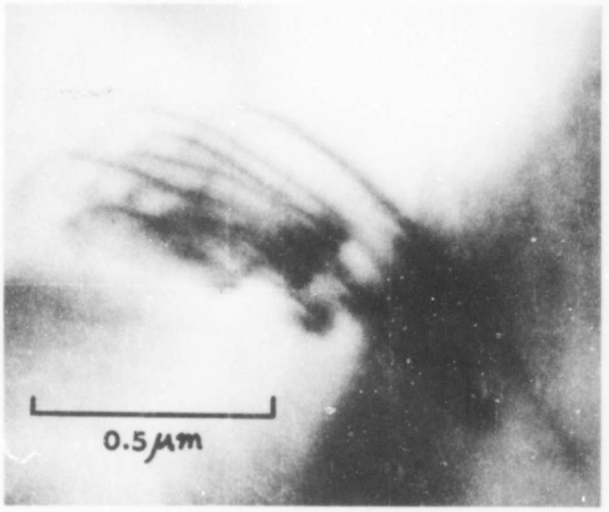

(e)

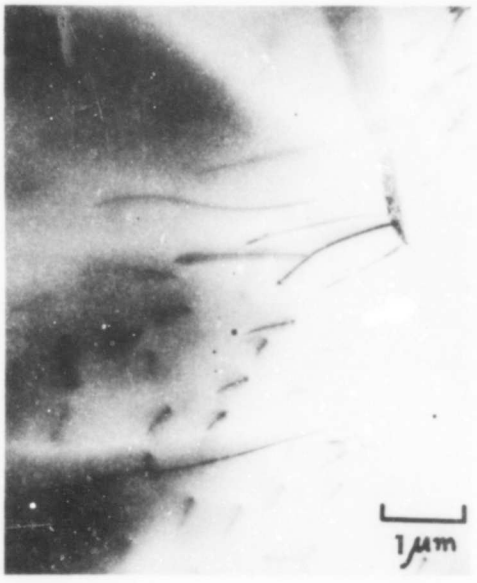

(f)

(g)

Figure 11 (continued)

These stepped dislocations, seen here in an intact grain within the bulk of a rather large fracture chip, have a strong resemblance to stepped cleavage textures frequently observed in fractographic studies of impacted alumina. Such dislocations, created during passage of an initial shock wave, may initiate cracks or dictate crack propagation paths during subsequent fragmentation in response to a reflected tension wave.

Defect Structures in Alumina Tile 7 After Ballistic Damage

In general, the substructure observed in this foil sample was almost similar to those observed from the foil described in the foregoing section. Figures 13 through 15 serve to illustrate some of its features. Bowed dislocations and dislocations at the tip of a crack are shown in Figures 13 and 14, respectively. Figure 15 shows a tangled mass of dislocations, having very high defect densities ($1 \times 10^{11}/cm^2$) of the sort commonly associated with heavily deformed metal crystals. This micrograph was taken from a foil representing a region where very extensive fracture occurred, apparently as a result of the reinforcement of shock waves reflected from the bottom and sides of the alumina tile. The transparent portion of the foil represents a very thin volume element lying about 20 μm beneath and approximately parallel to the actual fracture surface and normal to the impact axis.

Several sets of dislocations are involved in Figure 15. It is likely that two, perhaps three, different slip systems have been involved in producing the dislocation tangles. Tilting experiments on this foil using the invisibility criterion $g \cdot b = 0$ showed one set of dislocations (marked A) to have the Burgers vector $\langle 11\bar{2}0 \rangle$ type. Others could not be positively identified.

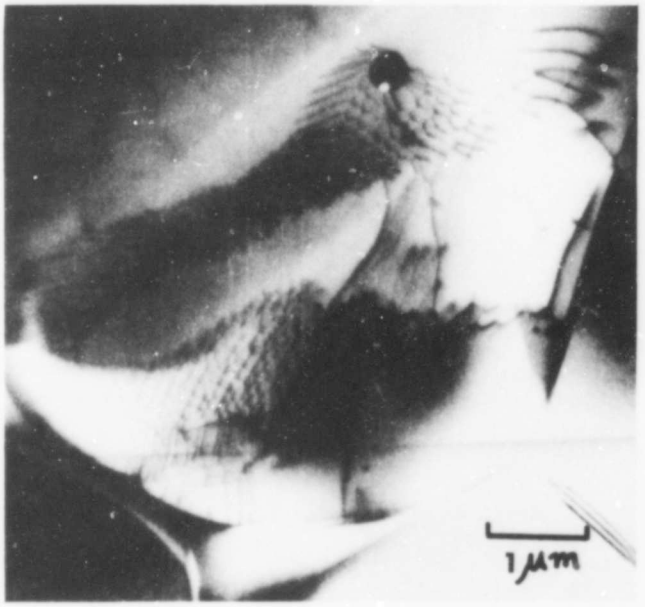

Figure 12. Transmission electron micrograph of foil thinned from bulk showing dislocation structures attributed to impact damage generated by plastic shock waves (tile 1, chip A, Figure 3a)

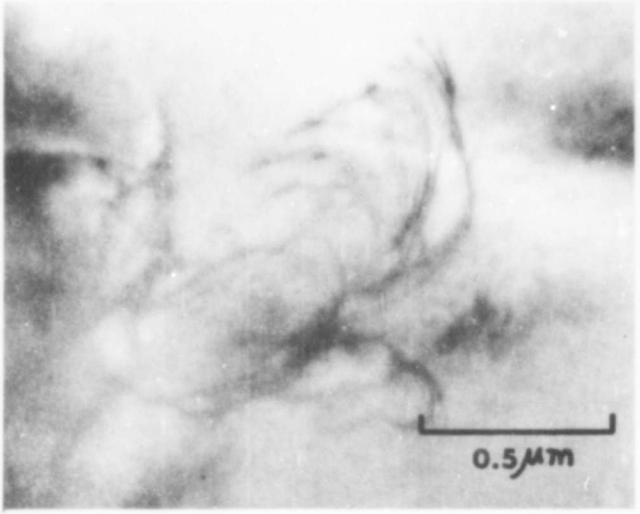

Figure 13. Bowed-out dislocations in ballistically damaged polycrystalline alumina (tile 7, chip E, Figure 3b)

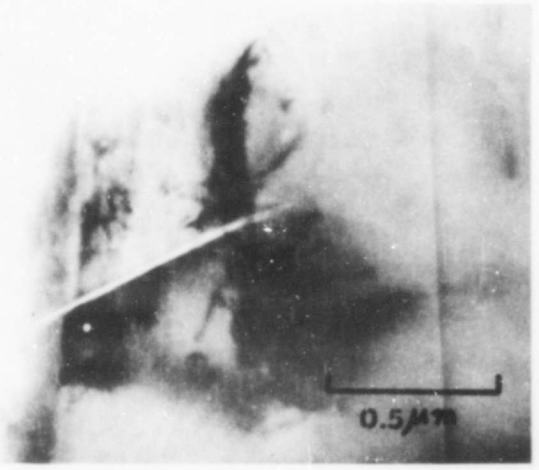

Figure 14. Defect structures associated with crack in ballistically damaged polycrystalline alumina (tile 7, chip E, Figure 3b)

Figure 15. Tangled mass of dislocations in ballistically damaged polycrystalline alumina (tile 7, chip E, Figure 3b)

These dislocations stand as evidence of significant amounts of localized plastic deformation occurring by slip at and near the crack tip. During the propagation of the crack, these shear processes created a plastically worked zone adjacent to the crack surface. On the basis of the evidence presented in Figure 15, this zone extends at least 20 μm (more than one grain diameter) into the bulk material. Tetelman (1962) has shown that plastic deformation accompanies a moving cleavage crack in silicon-iron single crystals and Johnson and Gibbs (1962) have produced similar evidence for germanium single crystals. Hockey (1970) reported that substantial quantities of plastic deformation by both slip and twinning took place during the placement of microhardness indentations in sapphire crystals and that high densities of dislocations were produced within the near surface regions by mechanical abrasion. The present observations are in agreement with, and provide additional strong and independent evidence in support of Congleton and co-workers findings (Congleton *et al.*, 1968, 1969) that the fracture surface energy of alumina had been substantially increased above the nominal free surface energy because of plastic work energy which had to be expended in deforming bulk material at and near an advancing crack front.

Ballistic Fracture Surface Topography with Scanning Electron Microscopy

By using the scanning electron microscope, a very good depth of field at reasonably high magnifications can be obtained. Figures 16 through 19 illustrate observations of a ballistically fractured polycrystalline alumina ceramic in the scanning electron microscope. In this instance, the electron beam had an accelerating potential of 25 kv, and specimens were examined directly without any previous

treatment except for vacuum deposition of a conductive thin film to avoid charging effects.

In general, the fracture surfaces are very rough and irregular. The path of the fracture is predominantly intergranular, but partly transgranular. Pores between grains and trapped pores within grains are readily noted, and considerable debris associated with the fracture process is present. These fragments are believed to have been formed during propagation of the main crack front as it spread on closely spaced, adjacent planes which subsequently joined by plastic tearing and/or fracture. Fragments are considered to result more from these latter processes than from the simple spreading of cleavage cracks.

A low magnification micrograph of the fracture surface is shown in Figure 16. Several pores between grains, internal cracks, cleavage fracture facets, and river marks are visible in this micrograph.

Figures 17 through 19 show typical features of transgranular fracture at somewhat higher magnifications. These micrographs give direct evidences of plastic deformation associated with the fracture surface and indicate clearly that fracture propagation is a very irregular process. These observations are consistent with earlier replication electron fractography studies reported by Palmour *et al.* (1969). In Figure 17, a peculiar "feathery" structure can be seen on the fracture surface. This illustrates the devious fracture path that the crack follows. During crack propagation (lower left - upper right axis), redirections of the fracture path formed irregular steps which serve to indicate fluctuations in the fracture velocity.

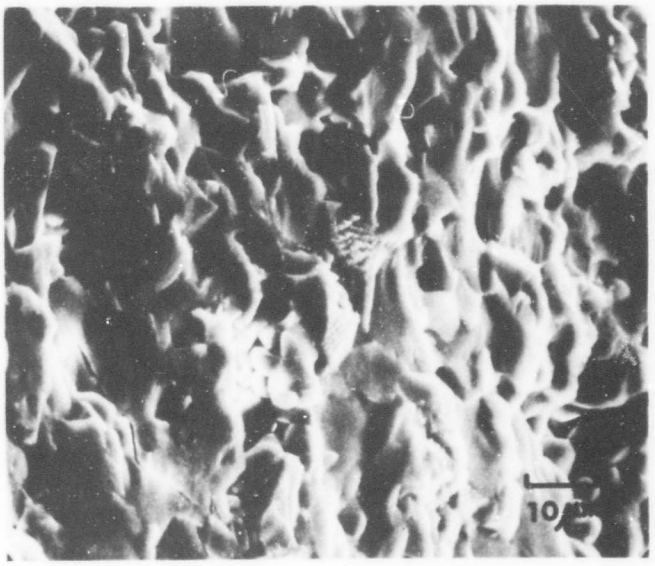

Figure 16. Scanning electron micrograph taken from a fracture surface of ballistically damaged alumina (tile 1, central impact region, Figure 3a); intergranular and transgranular fracture facets with internal crack path are visible

Figure 17. Scanning electron micrograph taken from a fracture surface of ballistically damaged alumina (tile 1, adjacent to chip B, Figure 3a); irregular steps formed by redirection of the fracture path; trapped pore is visible in the center of the micrograph

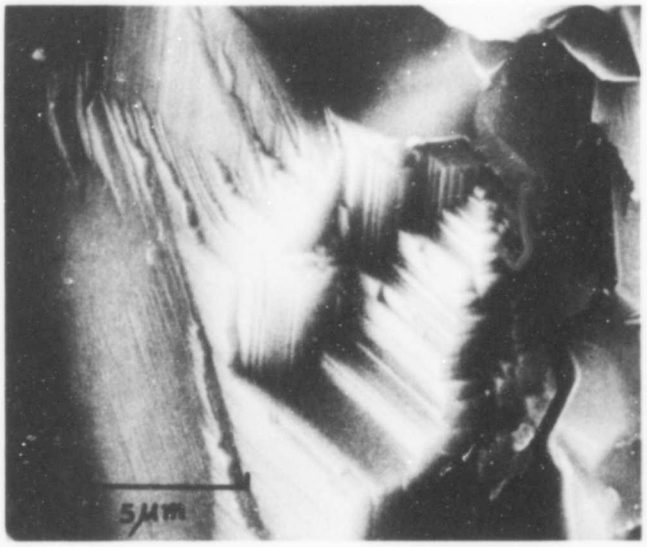

Figure 18. Scanning electron micrograph taken from a fracture surface of ballistically damaged alumina (tile 1, adjacent to chip B, Figure 3a); fine cleavage facets with internal crack path are visible

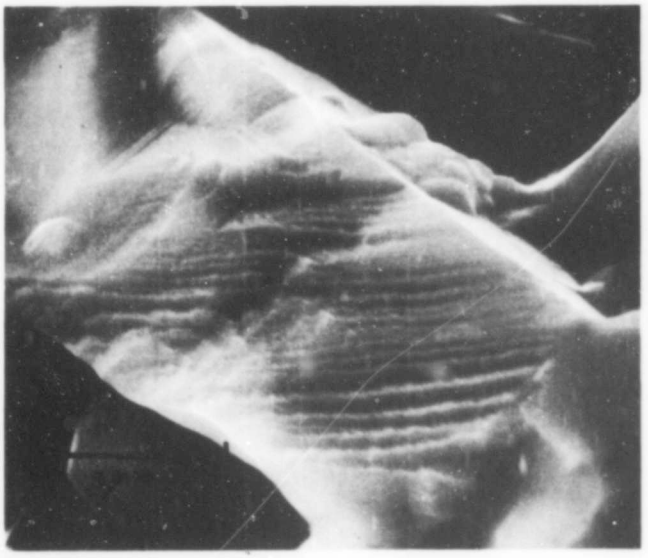

Figure 19. Scanning electron micrograph taken from a fracture surface of ballistically damaged alumina (tile 7, chip F, Figure 3b); adjacent cleavage planes are separated by regions of plastic tearing

The intersecting straight lines in Figure 17 are artifacts associated with electron beam damage to the pure Au conductive thin film during line profile scans. This sort of artifact is relatively rare in scanning microscopy and can be almost totally precluded by using the more stable Au-Pd alloy as the evaporant.

Heavily stepped and/or striated fracture textures characteristic of alumina's dominant rhombohedral cleavage mode (Palmour *et al.*, 1969) are illustrated in Figure 18 which also includes examples of other finer fracture markings. In Figure 19, less distinct cleavage steps in the lower portion, with finely textured, wavy, and obviously sheared regions near the upper left can be seen. From all these observations, it is apparent that the fracture process in polycrystalline alumina is not purely brittle. Instead, energy is absorbed during the propagation of fracture by any of several (often combined) processes, namely, secondary crack formation, localized plastic deformation, areal increases due to fracture surface roughness, and/or step formations which lead to high-energy tearing fracture.

DISCUSSION

As one part of an investigation whose earlier findings have been described by Palmour *et al.* (1969), this research documents in greater detail the role of inelasticity (microplasticity) as one of the significant processes occurring during fracture, fragmentation, and penetration of alumina ceramics during high velocity (ballistic) impact events. Detailed considerations of constitutive relations and/or kinematic interactions existing between an alumina ceramic tile (serving as the hard-face component in light-weight composite armor) and an impacting projectile are outside the scope of the present study. However, because they clearly reveal fundamental materials behavior during flow and fracture events at near-molecular levels, the present findings should have a significant bearing on further developments of suitable conceptual and mathematical forms for describing the dynamic response to impact of alumina and similar nominally brittle materials.

Alumina had been categorized as a truely brittle material only a decade ago. Although there were some evidences of dislocation-related flow in sapphire crystals associated with room temperature micro-indentation (Palmour, 1961; Palmour *et al.*, 1961a, 1961b) and abrasion (Stiejn, 1961), the ambient temperature fracture behavior of alumina had generally been treated on the basis of purely elastic response (Kingery and Coble, 1963; Stokes, 1964; Davidge, 1969) because of its complex crystal structure and its apparent inability to satisfy the von Mises-Taylor (Taylor, 1938) criteria of five independent shear modes for polycrystalline plasticity at room temperature. More recently, Congleton *et al.* (1968, 1969) have demonstrated an absence of true brittleness in

alumina below 1000° C with measurements of fracture surface energy, supported by direct observations of dislocations in thin fragments resulting from single fractures in alumina. Palmour *et al.* (1969) cited similar findings in ballistically damaged alumina, and Hockey (1970) confirmed extensive dislocation generation and motion during room temperature microindentation and abrasion of sapphire crystals.

The present investigation has revealed several optional and/or interrelated micromechanisms of fracture propagation in ballistically damaged alumina. At intermediate levels of magnification and resolution, scanning electron micrographs permit delineation of fine details of the fracture surface. The microstructural features are in large part those typical of nominally brittle fracture in polycrystalline materials; fracture surfaces are mainly composed of a combination of transgranular and intergranular regions (Figure 16). This indicates that the crack propagation mechanism is complex; it was necessary to propagate discontinuously, starting new cracks in succeeding grains. Such a process will tend to reduce the velocity of crack propagation and ultimately will stop crack advancement, unless high stress states are sustained by external loading. A halted crack in the interior of the bulk is visible in Figure 16. Transgranular fracture occurs in this view every three to four grain diameters (average grain size ~ 10 μm).

While the main crack propagates, bursts of easy cleavage spread ahead, become arrested and are reinitiated (Figure 17). Propagation of cleavage microcracks (discussed in detail for alumina in a previous paper, Palmour *et al.*, 1969) commonly results in the formation of complex cleavage facets (Figure 18), river patterns, and secondary cleavages, coupled with plastic tearing within individual grains

(Figure 19). Relatively easy cleavage processes spread forward and laterally through favorably oriented grains ahead of the main crack front; however, if the main crack is to advance, additional energy must be supplied by the available elastic strain energy. Some of it, an additive factor over and above the simple surface energy, is absorbed in the process of forming these fine extra textures.

Transmission electron microscopic examinations have shown a number of direct evidences of plastic deformation in the form of discrete dislocations, often interacted, as well as those which are piled up and tangled as in deformed metals. These examples of shear processes are localized rather than uniform in distribution. Even discounting the special experimental conditions (thinness, orientation) which must prevail to permit viewing them at all, the relative infrequency of reliable sightings suggests that their occurrence in truly heavy concentrations is probably dependent upon highly favorable combinations of grain orientations and stress-strain states. Hence they are related more or less directly to the special conditions of stress concentrations and geometric constraints occurring at a crack front.

Burgers vectors of dislocations associated with impact events have been determined in a limited number of cases from two-beam diffraction analyses. Both $\langle 11\bar{2}0 \rangle$ and $\langle 01\bar{1}1 \rangle$ types have been observed; in many instances both types are intermixed. The slip systems active under impact conditions are considered to be both basal, $(0001)\ [11\bar{2}0]$, and rhombohedral, $(10\bar{1}2)\ [\bar{1}011]$, in agreement with high temperature deformation studies in sapphire crystals, bicrystals and pure, dense polycrystalline alumina in which Becher (1970) identified specific slip

planes (single crystals and bicrystals) and determined similar Burgers vectors.

In earlier findings, Palmour *et al.* (1969) concluded that very significant quantities of energy were absorbed by plastic deformation occurring prior to and/or during fragmentation and propagation of cracks in bulk materials, as well as in fine particulates subjected to explosive or impact shock conditions. The present work clearly indicates that conditions for dislocation glide at some (if not all) crack tips have indeed been satisfied, even under high velocity ballistic impact conditions.

According to Martin (1969), a bullet of butter impacting a rigid material at 3000 ft/sec would generate pressures of around 125,000 psi at the impact point; the impact pressure is very much higher for a heavy and strong projectile. For the 0.30 caliber projectiles and impact velocities which produced the damage studied in this investigation, Martin's data suggest that the impact pressures were certainly in excess of 1×10^6 psi.

Presumably, flow in this nominally brittle material has been possible either as a consequence of very severe stress states resulting from locally intense stress concentrations or of shock-induced locally high temperatures of very short duration which might facilitate dislocation movement, or both. In either case, very strong and rather localized energy concentrations are certainly responsible for plastic flow in alumina ceramics.

LIST OF REFERENCES

Becher, P. F. 1970. Crystalline deformation and grain boundary behavior in aluminum oxide. Unpublished PhD thesis, Department of Materials Engineering, North Carolina State University at Raleigh, Raleigh, North Carolina. University Microfilms, Inc., Ann Arbor, Michigan.

Congleton, J., M. R. Holdsworth, and N. J. Petch. 1968. The brittle fracture of alumina. Final Technical Report, European Research Office, United States Army, Contract Number DAJA37-67-C-0522. University of Newcastle upon Tyne, England.

Congleton, J., and N. J. Petch. 1966. Dislocation movement in the brittle fracture of alumina. Acta Met. 14(10):1179-1182.

Congleton, J., N. J. Petch, and S. A. Shiels. 1969. The brittle fracture of alumina below 1000° C. Phil. Mag. 19:795-807.

Davidge, R. W. 1969. Mechanical properties of ceramic materials. Contemp. Phys. 10(2):105-124.

Friedel, J. 1959. Propagation of cracks and work hardening, pp. 498-523. *In* B. L. Averback, D. K. Felbeck, G. T. Hahn, and D. A. Thomas (eds.), Fracture. John Wiley and Sons, Inc., New York.

Gilman, J. J. 1956. Propagation of cleavage cracks in crystals. J. Appl. Phys. 27:1262-1269.

Gilman, J. J. 1958. Creation of cleavage steps by dislocation. Trans. Am. Inst. Min. metall. Eng. 212:310-315.

Gilman, J. J., W. G. Johnston, and G. W. Sears. 1958a. Dislocation etch pit formation in lithium fluoride. J. Appl. Phys. 29:747.

Gilman, J. J., C. Knudsen, and W. P. Walsh. 1958b. Cleavage cracks and dislocations in LiF crystals. J. Appl. Phys. 29:601-607.

Gleiter, H., E. Hornbogen, and G. Baro. 1968. Der mechanismus des korngrezen gleitens. Acta Met. 16:1053-1067.

Gorum, A. E., E. R. Parker, and J. A. Pask. 1958. Effect of surface conditions on room temperature ductility of ionic crystals. J. Am. Ceram. Soc. 41:161-164.

Griffith, A. A. 1920. Phenomena of rupture and flow in solids. Phil. Trans. Roy. Soc. 221A:163-198.

Gutshall, P. L., G. E. Gross, and G. D. Swanson. 1967. A study of the physical basis of mechanical properties of ceramics. Technical Report AFML-TR-67-99. Contract AF 33(615)-2669. Midwest Research Institute, Kansas City, Missouri.

Heuer, A. H., R. M. Cannon, and N. J. Tighe. 1970. Plastic deformation in fine-grain ceramics, pp. 339-365. *In* J. J. Burke, N. L. Reed, and V. Weiss (eds.), Ultrafine Grain Ceramics. Syracacuse University Press, Syracuse, New York.

Hirsch, P. B., A. Howie, R. B. Nicholson, D. W. Pashley, and M. J. Whelan. 1965. Electron Microscopy of Thin Crystals. Butterworths, London.

Hockey, B. J. 1970. Observations of plastic deformation in alumina due to mechanical abrasion. Am. Ceram. Soc. Bull. 49(4):498.

Howie, A., and M. J. Whelan. 1961. Diffraction contrast of electron microscopic images of crystal lattice defects: II. The development of a dynamical theory. Proc. Roy. Soc. A263:217-237.

Howie, A., and M. J. Whelan. 1962. Diffraction contrast of electron microscopic images of crystal lattice defects: III. Results and experimental confirmation of the dynamical theory of dislocation image contrast. Proc. Roy. Soc. A267:206-230.

Ishida, Y., and M. H. Brown. 1967. Dislocations in grain boundaries and grain boundary sliding. Acta Met. 15:857-860.

Johari, O. 1968. Comparison of transmission electron microscopy and scanning electron microscopy of fracture surfaces. J. of Metals 20:26-32.

Johari, O. 1969. Scanning Electron Microscopy/1969. IIT Research Institute, Chicago, Illinois.

Johnson, O. W., and P. Gibbs. 1962. Brittle fracture of germanium, pp. 315-338. *In* D. C. Drucker and J. J. Gilman (eds.), Fracture of Solids. Interscience Publishers, New York and London.

Johnston, T. L., C. H. Li, and R. J. Stokes. 1962. The strength of ionic solids, pp. 341-374. *In* American Society for Metals (editoral staff), Strengthening Mechanisms in Solids. American Society for Metals, Metals Park, Ohio.

Johnston, W. G., and J. J. Gilman. 1959. Dislocation velocities, dislocation density, and plastic flow in lithium fluoride crystals. J. Appl. Phys. 30:129.

Kim, C. H. 1969. River pattern cleavage steps on transverse secondary crack in ballistically damaged polycrystalline alumina. Am. Ceram. Soc. Bull. 48(8):830.

Kingery, W. D., and R. L. Coble. 1963. A review of the effect of microstructure on mechanical behavior of polycrystalline ceramics, pp. 103-113. Mechanical Behavior of Crystalline Solids. NBS Monograph No. 59, United States Government Printing Office, Washington, D. C.

Kolsky, H. 1953. Stress Waves in Solids. Oxford University Press, London.

Kolsky, H., and D. Rader. 1968. Stress waves and fracture, pp. 533-569. *In* H. Liebowitz (ed.), Fracture, Volume 1. Academic Press, New York and London.

Low, J. R. 1956. Dislocation and brittle fracture in metals, pp. 60-72. *In* G. Grammel (ed.), Deformation and Flow of Solids. Springer-Verlag, Berlin.

Low, J. R. 1959. A review of the microstructural aspects of cleavage fracture, pp. 68-90. *In* B. L. Averback, D. K. Felbeck, G. T. Hahn, and D. A. Thomas (eds.), Fracture. John Wiley and Sons, Inc., New York.

Martin, D. M. 1969. Penetration mechanics, pp. 5-12. *In* J. G. Dunleavy and W. H. Duckworth (eds.), Ceramic Armor Technology (DCIC Report 69-1, Part 1). Battelle Memorial Institute, Columbus, Ohio.

Nye, J. F. 1949. Plastic deformation of silver chloride. I. Internal stresses and glide mechanism. Proc. Roy. Soc. A198:191.

Orowan, E. 1948. Fracture and strength of solids. Repts. Prog. Phys. 12:185-232.

Palmour, H., III. 1961. Dislocations in single crystal sapphire as revealed by thermal etching. Unpublished PhD thesis, Department of Mineral Industries, North Carolina State University at Raleigh, Raleigh, North Carolina. University Microfilms, Inc., Ann Arbor, Michigan.

Palmour, H., III. 1964. Properties and applications of ceramic materials, pp. 793-832. *In* A. Standen (ed.), Kirk-Othmer Encyclopedia of Chemical Technology, Volume 4, Second Edition. John Wiley and Sons, Inc., New York.

Palmour, H., III, J. J. DuPlessis, and W. W. Kriegel. 1961a. Microstructural features and dislocations on thermally etched sapphire surfaces. J. Am. Ceram. Soc. 44(8):400-404.

Palmour, H, III, C. H. Kim, D. R. Johnson, and C. E. Zimmer. 1969. Fractographic and thermal analyses of shocked alumina. Technical Report 69-5. Office of Naval Research, Contract N00014-68-A-0187. North Carolina State University at Raleigh, Raleigh, North Carolina.

Palmour, H., III, W. W. Kriegel, and J. J. DuPlessis. 1961b. Microbrittleness anisotropy in thermally etched sapphire, pp. 313-331. *In* W. W. Kriegel and H. Palmour, III (eds.), Mechanical Properties of Engineering Ceramics. Interscience Publishers, Inc., New York.

Parker, E. R. 1961. Ductility of magnesium oxide, pp. 65-87. *In* W. W. Kriegel and H. Palmour, III (eds.), Mechanical Properties of Engineering Ceramics. Interscience Publishers, Inc., New York.

Patterson, R. L., and H. G. F. Wilsdorf. 1968. Experimental observations of dislocations, pp. 183-242. *In* H. Liebowitz (ed.), Fracture, Volume 1. Academic Press, New York and London.

Rinehart, J. S. 1951. Some experimental indications of the stresses produced in a body by an exploding charge. J. Appl. Phys. 22(9): 1178-1181.

Scheuplein, R. J., and P. Gibbs. 1960. Surface structure in corundum: I. Etching of dislocation. J. Am. Ceram. Soc. 43(9):458-472.

Smallman, R. E., and K. H. G. Ashbee. 1966. Modern Metallography. Pergamon Press, New York.

Steijn, R. P. 1961. On the wear of sapphire. J. Appl. Phys. 32(10): 1951-1958.

Stokes, R. J. 1964. Correlation of mechanical properties with microstructure, pp. 41-72. Microstructure of Ceramic Materials. NBS Misc. Publication 257. United States Government Printing Office, Washington, D. C.

Stokes, R. J., T. L. Johnston, and C. H. Li. 1958. Crack formation in magnesium oxide single crystals. Phil. Mag. 3(31):718-725.

Stroh, A. N. 1955. The formation of cracks as a result of plastic flow. Proc. Roy. Soc. A232:548.

Swanson, G. D., and G. E. Gross. 1968. Physical parameters affecting fracture strength and fracture mechanisms in ceramics. Final Report, United States Navy, Naval Air Systems Command, Contract No. N00019-68-C-0127, Midwest Research Institute, Kansas City, Missouri.

Taylor, G. I. 1938. Plastic strain in metals. J. Inst. Metals 62: 307-324.

Tetelman, A. S. 1962. The plastic deformation at the tip of a moving crack, pp. 461-501. *In* D. C. Drucker and J. J. Gilman (eds.), Fracture of Solids. Interscience Publishers, Inc., New York and London.

Thornton, P. R. 1968. Scanning Electron Microscopy. Chapman and Hall, Ltd., London.

Tighe, N. J. 1970. Microstructure of fine-grained ceramics, pp. 109-133. *In* J. J. Burke, N. L. Reed, and V. Weiss (eds.), Ultrafine Grain Ceramics. Syracuse University Press, Syracuse, New York.

Tighe, N. J., and A. Hyman. 1968. Transmission electron microscopy of alumina ceramics, pp. 121-136. *In* F. W. Vahldiek and S. A. Merson (eds.), Anisotropy in Single-Crystal Refractory Compounds. Plenum Press, New York.

Wiederhorn, S. M. 1969. Fracture of sapphire. J. Am. Ceram. Soc. 52(9):485-491.